Composites Science and Technology 117 (2015) 146–158

Contents lists available at ScienceDirect

Composites Science and Technology

journal homepage: http://www.elsevier.com/locate/compscitech

Improving the toughness and electrical conductivity of epoxy nanocomposites by using aligned carbon nanofibres

Raj B. Ladani [a], Shuying Wu [a], Anthony J. Kinloch [b], Kamran Ghorbani [a], Jin Zhang [c], Adrian P. Mouritz [a], Chun H. Wang [a, *]

[a] Sir Lawrence Wackett Aerospace Research Centre, School of Aerospace, Mechanical & Manufacturing Engineering, RMIT University, GPO Box 2476, Melbourne, VIC 3001, Australia
[b] Department of Mechanical Engineering, Imperial College London, South Kensington Campus, London SW7 2AZ, UK
[c] Institute for Frontier Materials, Deakin University, Geelong Waurn Ponds Campus, VIC 3220, Australia

ARTICLE INFO

Article history:
Received 5 April 2015
Received in revised form
6 June 2015
Accepted 9 June 2015
Available online 18 June 2015

Keywords:
A. Adhesive joints
B. Fracture toughness
C. Modelling
C. Fibre bridging
Fibre pull-out

ABSTRACT

There is an increasing demand for high performance composites with enhanced mechanical and electrical properties. Carbon nanofibres offer a promising solution but their effectiveness has been limited by difficulty in achieving directional alignment. Here we report the use of an alternating current (AC) electric field to align carbon nanofibres in an epoxy. During the cure process of an epoxy resin, carbon nanofibres (CNFs) are observed to rotate and align with the applied electric field, forming a chain-like structure. The fracture energies of the resultant epoxy nanocomposites containing different concentrations of CNFs (up to 1.6 wt%) are measured using double cantilever beam specimens. The results show that the addition of 1.6 wt% of aligned CNFs increases the electrical conductivity of such nanocomposites by about seven orders of magnitudes to 10^{-2} S/m and increases the fracture energy, G_{Ic}, by about 1600% from 134 to 2345 J/m^2. A modelling technique is presented to quantify this major increase in the fracture energy with aligned CNFs. The results of this research open up new opportunities to create multi-scale composites with greatly enhanced multifunctional properties.

1. Introduction

Thermosetting epoxy polymers are widely used in aerospace and automotive applications as matrices for manufacturing fibre reinforced composites and as adhesives for joining structural components. Despite offering many desirable properties, thermosetting polymers typically exhibit a low electrical conductivity and a low fracture toughness, which leads to poor resistance to lightning strike and crack growth [1]. In the absence of any through-thickness reinforcement, fibre composites and bonded joints are susceptible to delamination or debonding [2]. The low electrical conductivity of composites and bonded structures, especially along the thickness direction, present challenges in protecting of aircraft against lightning strikes and electromagnetic interference. Also, good electrical conductivity is needed to meet fire retardant anti-static regulations for mining equipment, and oil-gas storage and transportation. Hence, improving the through-thickness toughness and electrical conductivity of fibre composites is of great importance.

Traditional techniques to improve the through-thickness properties and damage tolerance of epoxy polymers are to form a polymeric alloy via the addition of thermoplastics [3,4] or rubber tougheners [5,6]. Although these methods provide significant improvements to the toughness, the electrical conductivity remains unchanged because such additives are dielectric. More recently, studies on conductive carbon-based nanofillers, such as carbon nanotubes (CNTs) [7–9], carbon nanofibres (CNFs) [10–12] and graphene nanosheets (GNSs) [13,14], have shown significant promise to increase the toughness of epoxy polymers, as well as the ability to improve their electric conductivity. A number of studies have reported good improvements in toughness of epoxy nanocomposites by the addition of CNTs [15–18] or CNFs [12,19,20]. For example, Tang et al. [21] reported that the addition of 1 wt% CNTs increased the fracture energy of an epoxy by about 130%. Palmeri et al. [22] showed that the addition of just 0.68 wt% CNFs improved the fracture toughness of an epoxy by about 43–112%. Similarly, other studies have reported fracture toughness improvements

* Corresponding author.
E-mail address: chun.wang@rmit.edu.au (C.H. Wang).

http://dx.doi.org/10.1016/j.compscitech.2015.06.006

between 40 and 80 % for CNT or CNF modified epoxy nanocomposites. While these improvements are impressive, they are significantly lower than the nine fold increase in fracture toughness reported for nano-silica [23] and rubber-toughened modified epoxy polymers [24]. But the use of carbon based nanofillers can simultaneously increase the electric conductivity and mechanical properties, unlike nano-silica and rubber particles.

One major factor limiting the property improvements achieved to date in epoxy nanocomposites has been the fact that the carbon nanofillers are typically randomly-oriented, which arises naturally from the dispersion process using ultrasonication and/or mechanical mixing [25]. Unsurprisingly, the improvements achieved in many important properties of the epoxy nanocomposites containing randomly-oriented carbon-based nanofillers are significantly lower than what would be predicted had the nanofillers been aligned in the desired direction, albeit that the properties are now of course anisotropic. Theoretical modelling and computational simulations suggest that aligning nano-scale structures (e.g. CNTs and CNFs) in a certain direction should lead to substantial advantages compared with randomly-oriented nanofillers. Indeed, numerical analyses have confirmed that 1.0 vol% aligned CNTs should increase the stiffness of an epoxy by about 300% [26] in the alignment direction. Similarly, the alignment of 3.0 vol% CNTs in epoxy normal to the crack growth plane is predicted to enhance the toughness by up to 400% [27]. Unfortunately, there is a dearth of suitable processes to align carbon nanofillers along the through-thickness direction of composites. However, recently the use of electric- and magnetic-fields to align nanoparticles in liquid resins, prior to curing, has been reported [28–32]. The present authors have shown that by attaching nano-magnetite (Fe_3O_4), CNFs can be aligned by using a very weak (0.05T) magnetic field [32]. Under the application of an electric field between a pair of parallel plate electrodes, the nanofillers may align to form a chain-like network in the direction of the electric field [33]. This mechanism of the self-aligning of conductive carbon nanofillers in polymers offers a new opportunity to create multi-scale structures. Since thermosetting resins, such as epoxy resins, may typically possess a relatively low viscosity prior to cure, the application of an electric- and/or magnetic-field will be able to transform the randomly-oriented carbon-based nanofillers to give a highly aligned structure. Upon curing, the aligned nanofillers will remain in place in the resulting epoxy nanocomposite.

The alignment of CNFs [33] and CNTs [16] using an electric field has indeed been reported to improve the electrical conductivity of polymers through the formation of a percolating network at extremely low weight fractions of the added CNFs or CNTs. Khan et al. [16] has reported an additional 30% increase in the fracture toughness of CNT modified epoxy nanocomposites due to the alignment of the CNTs normal to the crack growth plane using a direct current (DC) electric field. Although randomly aligned CNFs have also been reported [22] to improve the fracture toughness of nanocomposites, the effect of their alignment on the fracture energy has never been studied.

Considering that CNFs may be an excellent alternative to CNTs due to their wide availability and lower cost [34], the present study focuses on dual improvements in the electrical conductivity and fracture toughness of an epoxy nanocomposite containing aligned CNFs. The alignment is accomplished by applying an external AC electric-field whilst the resin is liquid prior to crosslinking. Upon curing the epoxy resin, the resultant epoxy nanocomposite contains aligned CNFs. The effects of alignment of the CNFs on the fracture toughness and electrical conductivity of the epoxy nanocomposite are measured and theoretical modelling studies are undertaken to quantify the increase in the fracture toughness due to the alignment of the CNFs. The results are then compared to the values pertinent to the unmodified epoxy and the epoxy nanocomposites containing randomly-oriented CNFs.

2. Materials and experimental methodology

2.1. Materials

The epoxy resin used was a liquid blend of bisphenol A and bisphenol F ('105' from West System) and the hardener ('206' from West System) was a blend of aliphatic amines and aliphatic amine adducts based on diethylenetriamine and triethylenetetramine. Commercially-available vapour-grown carbon nanofibres, Pyrograf® – III PR-24-HHT and supplied by Applied Sciences Inc., USA, were employed as the nanofiller. The CNFs had a diameter of about 70–200 nm and a length of 50–200 μm [35]. Carbon fibre composite substrates were manufactured using 12 plies of unidirectional T700 carbon-fibre/epoxy-prepreg (VTM 264 supplied by Applied Composites Group). The substrates, with dimensions of 300 mm × 250 mm × 2.5 mm, were cured and consolidated in an autoclave at 120° C for 1 h, in accordance with the manufacturer's recommended cure process. The substrate surfaces were abraded using 320 grit aluminium oxide abrasive paper, cleaned under running tap water for about 2 min, degreased with acetone, and finally cleaned with distilled water to remove any surface impurities. The substrates were then used as the electrodes between which the liquid epoxy resin mixed with the CNFs, prepared according the procedure described below, acted as an adhesive layer.

2.2. Dispersion and in-situ alignment of the CNFs in the liquid epoxy resin

A three-roll mill (Dermamill 100) was used to disperse the CNFs in the liquid epoxy resin. Firstly, 1.0 wt% of the CNFs were hand mixed with dispersion-aiding additives based upon solvent-free acrylate copolymers, namely Disperbyk-191 and -192 (supplied by BYK®). The dispersive surfactants that were added to the CNFs were equal to the weight of the CNFs, resulting in a mixture of CNFs:D-191:D-192 at weight ratio of 1:1:1. The CNF-surfactant mixture was then added to the epoxy resin, with no curing agent yet added, and hand mixed for 5 min. This mixture was then passed four times through the three-roll mill at 150 rpm with varying gap sizes. In order to achieve a homogeneous dispersion of CNFs, with each subsequent pass the mill gap size was gradually reduced until the smallest gap setting of 20 μm had been reached. The 1.0 wt% CNF/epoxy mixture was then diluted by adding epoxy resin, to achieve the desired weight fraction of CNFs (0.1%, 0.4%, and 0.7%) in the epoxy resin. A batch of 1.6 wt% CNFs was mixed and dispersed separately following the above procedure, due to its relatively higher weight fraction in the epoxy resin.

To observe the AC electric-field induced alignment of the CNFs, a 0.1 wt% CNF/epoxy resin mixture was placed on a glass slide between two parallel carbon electrodes with a 2.0 mm separation distance. VTM264 carbon fibre-epoxy prepreg strips were used as electrodes. An AC signal generator (Tektronix CFG250) in combination with a wideband amplifier (Krohnhite 7602M) was used to apply 60 V AC at 10 kHz to generate the AC electric field of 30 V/mm strength. The *in-situ* alignment of the CNFs in the liquid epoxy resin was observed using a Leica optical microscope. Time-lapsed images of the CNFs were acquired using a Leica DC 300 digital camera to observe the alignment of the CNFs in the epoxy resin. The distribution of the orientation angles of the CNFs was ascertained using the Leica image processing software.

2.3. Joint manufacturing and testing

The surface-treated carbon-fibre composite substrates (150 × 250 × 2.5 mm) were placed between glass fibre frames which were used as a dam to prevent the epoxy mixture from flowing out of the joint. Spacers, 2 mm in thickness made of glass slides, were placed at both ends of the joint to control the thickness of the epoxy layer between the substrates. Teflon-coated tape about 30 mm long and 11 μm thick was placed at an approximately equal distance between the two substrates, at one end of the joint, to act as a crack starter. The amine-based curing agent was added to the dispersed CNF/epoxy resin mixture and hand-mixed for approximately 5 min. This CNF-modified epoxy resin mixture was then poured between the substrates. Such bonded joints were prepared using the epoxy nanocomposite as the adhesive layer for six different concentrations of CNFs (i.e. 0.0, 0.1, 0.4, 0.7, 1.0 and 1.6 wt %). Studies were undertaken for two different orientations of the CNFs (i.e. randomly-oriented and aligned). In order to achieve a highly aligned network of CNFs in the through-thickness direction of the epoxy nanocomposite layer, an AC electric field of 30 V/mm at 10 kHz was applied between the carbon-fibre composite substrates during the initial 1 h period of the curing cycle of the epoxy resin. The epoxy resin was then cured at room temperature (i.e. 25 °C) for 48 h in total to form the epoxy nanocomposite. After this time period, the CNF epoxy nanocomposite is referred to as 'n Random' or 'n Aligned', where 'n' refers to the amount of CNF by percentage weight of the total epoxy resin followed by the orientation. The joints were then cut into 20 mm wide double-cantilever beam (DCB) adhesively-bonded specimens. The electrical conductivity of the cured joints was tested using an impedance analyser (HP4192A). Fig. 1 shows a schematic of the DCB specimen. A sharp crack tip was achieved by carefully wedging the crack opening from the tip of the Teflon film. A minimum of five DCB specimens were tested in a 10 kN Instron machine at a crosshead speed of 1 mm/min in accordance with ISO 25217 [36]. The load versus displacement curves were recorded continuously, and a travelling optical microscope was used to observe the crack length in the epoxy nanocomposite layer. The mode I fracture energy, G_{Ic}, was calculated based on 'corrected beam theory' [36]. The crack was always found to propagate cohesively through the epoxy nanocomposite layer itself.

3. Results and discussion

3.1. Dispersion and in-situ alignment studies

The as-supplied CNFs were in the form of agglomerates, as shown in Fig. 2a. The use of the three-roll milling method was efficient at breaking up the agglomerates and dispersing the CNFs, as may be seen from Fig. 2b. The diameter of the as supplied CNFs was measured from five different SEM micrographs (see Fig. 2a) with a total CNF population equal to 510. As shown in Fig. 2c, the diameter distribution of the CNFs has a range from 60 nm to 200 nm with a lognormal peak of about 95 nm. The post-dispersion length of CNFs in the epoxy resin was measured using the Leica image processing software. Fig. 2d shows the length distribution of the CNFs after three-roll milling. The three-roll mill dispersion resulted in sizes of the CNFs ranging from 2 to 50 μm, with the majority of the CNFs having lengths of 16–24 μm. Dispersion using ultrasonication or three-roll milling would inevitably reduce the length of CNFs, however three-roll milling has been reported to be less damaging [25]. Retaining a relatively long length for the CNFs during their dispersion in the epoxy is considered to be important for obtaining an effective toughening of the epoxy nanocomposite, since the theoretical improvement in the fracture energy of the epoxy, from a fibre pull-out mechanism, will be proportional to the square of half the embedded length of the CNFs [37].

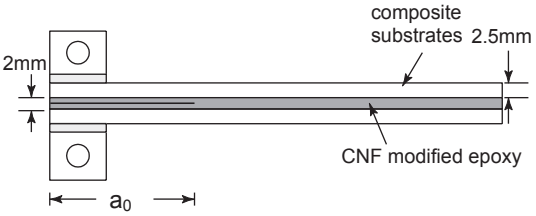

Fig. 1. Schematic of the double-cantilever beam (DCB) joint configuration.

The response of the CNFs in the liquid epoxy resin to the AC electric field was verified through *in-situ* optical microscopy. An AC electric field with an amplitude of 30 V/mm at 10 kHz was applied to 0.1 wt% of CNFs dispersed in the epoxy resin (i.e. containing no curing agent). Observations using the optical microscope were made to measure the time to achieve alignment. Fig. 3a shows an optical micrograph for t = 0 min (i.e. before the application of the AC electric field) and, therefore, the CNFs are randomly-oriented. Upon application of the AC electric field the CNFs rotated to align in the direction parallel to the electric field, as shown in Fig. 3b. For a 30 V/mm electric-field strength, the time needed to complete the alignment process was found to be about 5 min; beyond which no further improvement in the degree of alignment was observed. Fig. 3c shows a comparison of the angle distribution between the randomly-oriented CNFs (i.e. no electric field was applied) and the CNFs where the AC electric field was applied for 5 min. The use of the AC electric field has resulted in 85% of the CNF population of being aligned within ±15° of the applied electric-field direction. As shown in Fig. 4, the orientation of the CNFs was further verified using transmission electron microscopy to view 90 nm thick slices (obtained through ultramicrotomy) of the epoxy nanocomposite. The alignment of the CNFs can be attributed to the *dielectrophoresis* process, which is widely used for electrophoretic deposition of particles [38]. In the dielectrophoresis process, a particle immersed in a dielectric medium undergoes polarization when subjected to an externally applied electric field. This arises from the difference in the dielectric properties and the electrical conductivities between the particle and the medium. For one-dimensional particles, such as CNFs and CNTs, due to their shape anisotropy the longitudinal polarizability is at least an order of magnitude greater than the transverse polarizability [39,40]. Therefore, when subjected to an electric field, the difference in polarizability of the CNFs results in an induced dipole and its interaction with the electric-field gradient generates a torque resulting in rotation of the long axis of CNFs, so causing them to align along the external-field direction [41].

3.2. Electrical conductivity studies

Fig. 5a shows a logarithmetic versus logarithmetic plot of the electric conductivity (or specific conductance) as a function of frequency of the epoxy nanocomposite layer in the bonded joint in the direction normal to the substrate surfaces, i.e. in the through-thickness direction. The '0.1 random' epoxy nanocomposite (0.1 denotes the wt% of CNFs present) reveal an increase in the capacitive component with increasing frequency, similar to that of the unmodified (i.e. 'neat') epoxy polymer. While for the '0.1 aligned' case, there is always at least one order of magnitude improvement in the conductivity below about 1 kHz, independent of the frequency. This is then followed by a region of somewhat increasing conductivity which is similar in value to that of the '0.1 random' samples. A similar trend was also observed for the '0.4 random'

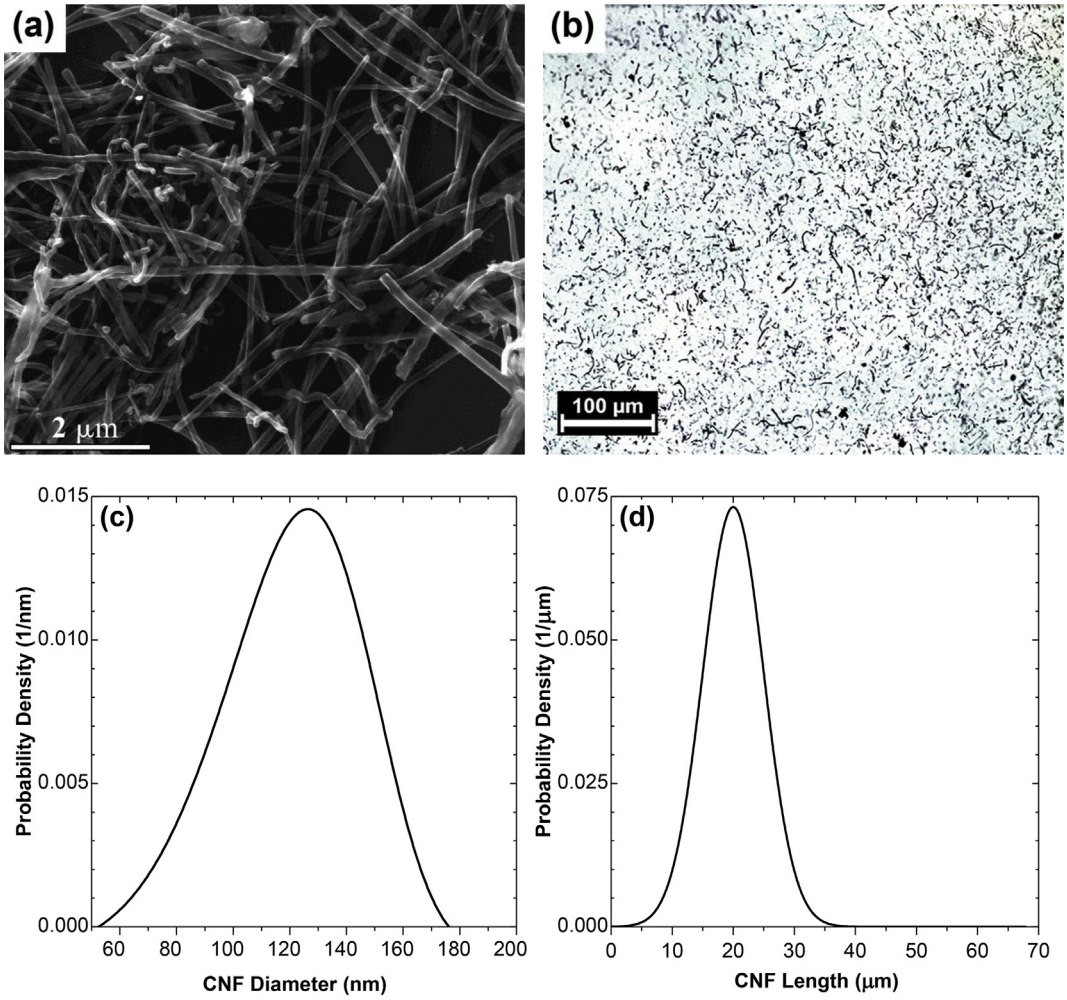

Fig. 2. (a) SEM micrograph of the as supplied CNF and (b) optical micrograph of the epoxy resin/0.1 wt% CNF mixtures after three-roll mill dispersing; (c) diameter probability density function of the as supplied CNFs measured from SEM micrograph and (d) length probability density function of the CNFs after the three roll-milling dispersion process from Fig. 2b.

epoxy nanocomposite with a frequency-independent conductivity up to about 10 kHz. This can be explained by considering the complex frequency dependent conductivity response of conductor-dielectric nanocomposites that are often analysed in terms of the *resistance-capacitance (R–C)* model,

$$\sigma(\omega) = \sigma_{dc} + \sigma_{ac} = \sigma_0 + A\omega^n \quad (1)$$

where σ_{dc} and σ_{ac} are the DC and AC conductivity respectively, ω is the angular frequency, A is a constant and the exponent n is in a range between 0 and 1 depending on the frequency range [42]. The AC component of the conductivity corresponds to the power-law frequency dependence and is well known for a wide range of materials which was noted by Jonscher [43] as the "Universal Dielectric Response". For each composition of nanocomposite containing a conductive filler, the above conductivity relationship is governed by a critical frequency,ω_c below which the conductivity becomes frequency-independent (i.e. DC conductivity, σ_{dc} when $\omega \rightarrow 0$), and beyond which the power-law is followed. Curve fitting the AC conductivity results of the neat epoxy composite using Eq. (1), the following values are obtained: $A = 1.5 \times 10^{-8}$ and $n = 1.0$, as shown in Fig. 5a. It is interesting to note that Eq. (1) with these two values is in good agreement with the other loadings of CNFs. The appearance of a DC plateau for the '0.1 aligned' and '0.4 random' samples below their critical frequencies of 1 kHz and 10 kHz, respectively, indicates a transition from an insulating to a conducting regime, which reflects the formation of some percolating CNF networks. However, for the '0.1 random' sample, the absence of the DC plateau region indicates that the conductivity is dominated entirely by the dielectric property of the epoxy. By contrast, the conductivity of '0.4 aligned' samples is significantly higher than that of the '0.4 random' samples and is independent of the frequency over the complete range of frequencies that were investigated. This indicates that the conductivity of the '0.4 aligned' nanocomposite is dominated by the conductor (i.e. the CNF networks) for most part. With further increases in the concentration of CNFs, the conductivity was found to be frequency-independent for both the randomly-oriented and the aligned nanocomposites, and increased to a maximum value of 10^{-2} S/m for the '1.6 aligned' epoxy nanocomposite. The measured increase in the DC conductivity of the epoxy as a function of the weight fraction of CNFs is shown in Fig. 5b.

From these results, the increases in the conductivity suggest that a network of percolated nanofibres formed at a concentration of CNFs above about 0.7 wt% when they were randomly-oriented. However, the application of the AC electric field during the curing of the epoxy resin resulted in alignment of the CNFs and it appears that the percolation network now formed at a concentration of

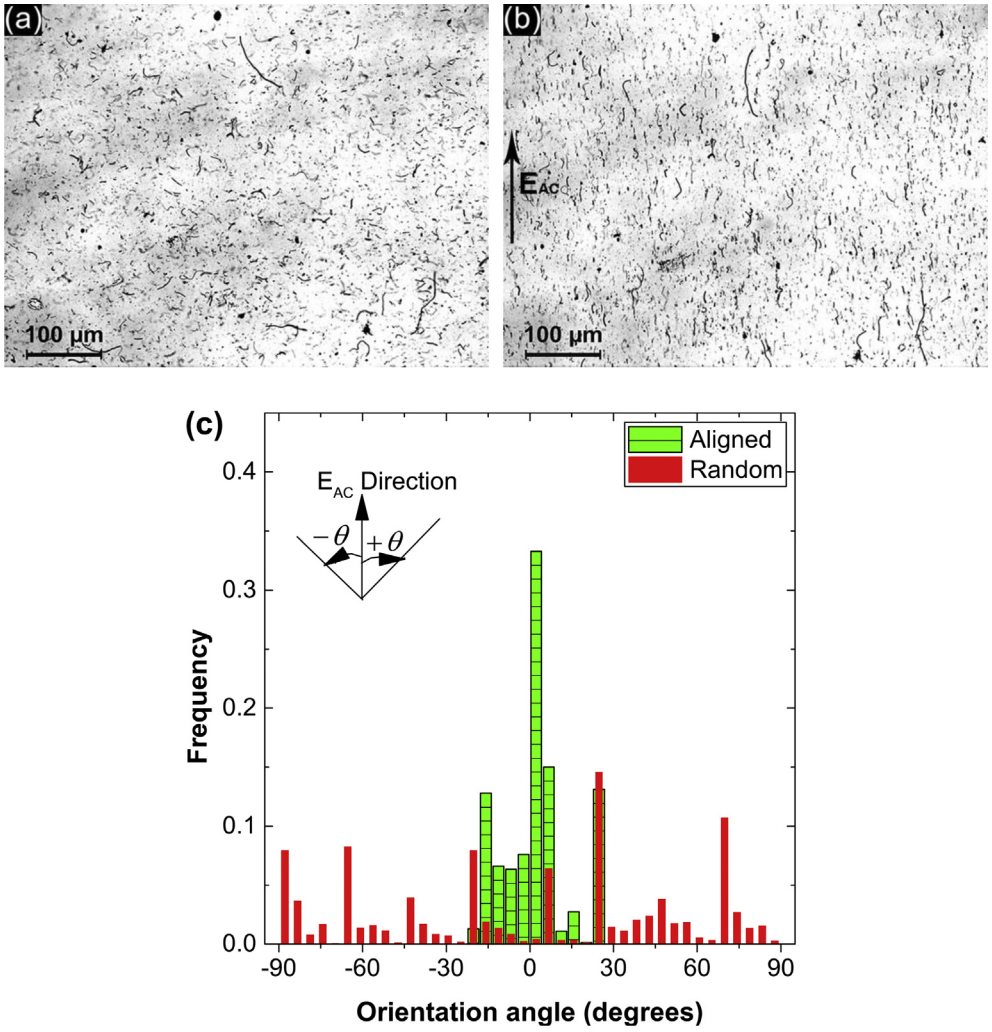

Fig. 3. *In-situ* alignment of 0.1 wt% CNFs in the epoxy resin using the AC electric field (a) t = 0 min (i.e. randomly-oriented CNFs) and (b) t = 5 min (i.e. aligned CNFs), the direction of the applied AC electric field is indicated by the arrow; (c) comparison of the angle distribution of the randomly-oriented CNFs (from Fig. 3a) and the CNFs aligned after being subjected to the AC electric field for 5 min (from Fig. 3b).

CNFs of about 0.4 wt%. A comparison of these results with the DC conductivity of these nanocomposites gave identical results. Indeed, the advantage of aligning the CNFs in the epoxy nanocomposites is clearly apparent from the '0.7 aligned' samples, which had a higher conductivity than the '1.0 random' samples. However, for the 1.6 wt% samples, the increase in the conductivity of the epoxy nanocomposites due to the alignment of CNFs was minimal. This is attributed to the lack of free space available for the

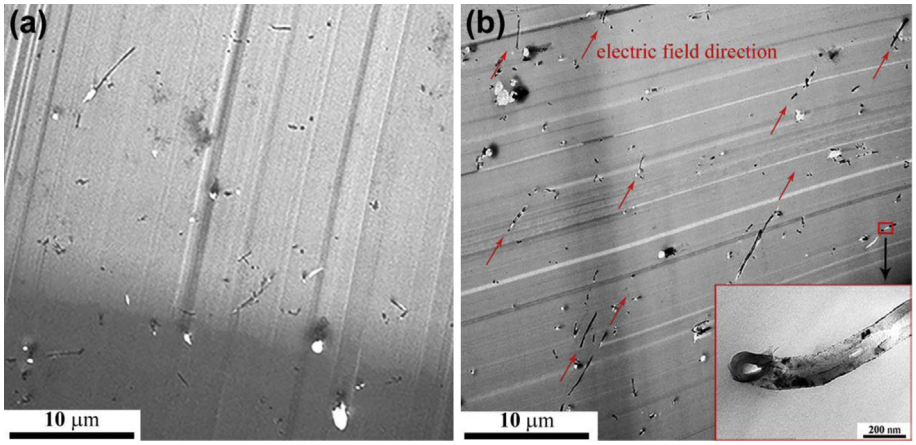

Fig. 4. TEM images of the epoxy nanocomposites. (a) 0.7 wt% of CNFs and randomly-oriented. (b) 0.7 wt% of CNFs and aligned via the application of the AC electric field for 5 min (The arrows indicate the direction of the applied AC electric field.) Inset shown in (b) gives a detailed view of CNF.

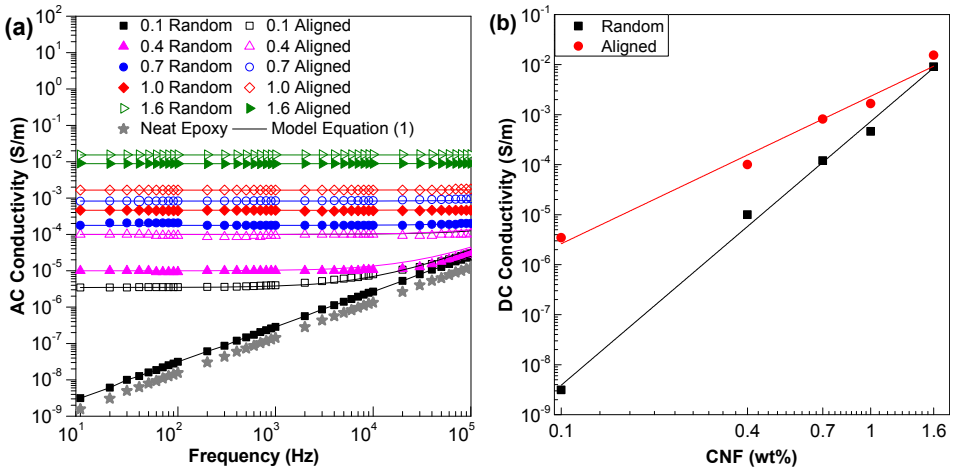

Fig. 5. (a) Electrical conductivity of the epoxy nanocomosites as a function of frequency. (a) AC conductivity as a function of frequency; all solid lines are calculated from Equation (1). (b) DC conductivity as a function of CNF concentration for both randomly-oriented or aligned CNFs in the epoxy nanocomposites; the lines represent a linear fit. (Note: The conductivity of the aligned nanocomposites was measured in the direction of alignment.)

CNFs to rotate in the direction of the electric field due to the resistance from the interaction between closely packed CNFs [44] and the likely formation of CNF agglomerates in the epoxy at these relatively high weight fractions of CNFs.

3.3. Fracture energy studies

As shown in Fig. 6, the applied load versus crack opening displacement curves for the DCB tests with the adhesive layer comprising of unmodified epoxy or epoxy nanocomposites containing randomly-oriented or aligned CNFs all revealed that the type of crack growth was unstable, i.e. stick-slip, in nature, with the distinct "saw-tooth" shaped load versus displacement curves typical of such failure. The maximum peak loads of these curves corresponded to the onset of crack growth, while the lower values of load corresponded to the arrest of the fast propagating crack. For the DCB specimens with a higher weight concentration of CNFs in the epoxy nanocomposite layer, the length of the unstable crack growth was much greater, due to the higher maximum loads for crack propagation that were attained. Therefore, the load versus displacement curves for these samples had fewer peaks. The values of G_{Ic} for the onset of crack propagation were calculated using the maximum loads that were measured [35]. The locus of failure was along the centre of the unmodified (i.e. neat) epoxy polymer or epoxy nanocomposite layer in all cases.

The results of the fracture toughness tests of the DCB tests with the adhesive layer comprising of unmodified epoxy or epoxy nanocomposites containing randomly-oriented or aligned CNFs are shown in Fig. 7. The average mode I fracture energy, G_{Ic}, of the unmodified epoxy layer for the DCB joint was found to be 134 J/m^2, as would be expected for a relatively brittle epoxy. An increase in the value of the fracture energy was observed for all the epoxy nanocomposites. For the nanocomposites, the fracture energy increases almost linearly with the concentration of CNFs. In addition, a somewhat greater improvement in the fracture energy was consistently measured for samples containing aligned CNFs, with their orientation of course normal to the direction of crack growth. The '1.6 aligned' specimen showed the highest improvement, with a sixteen fold increase in the fracture energy compared to the unmodified epoxy. Further, compared to the nanocomposites containing randomly-oriented CNFs, the alignment of the CNFs resulted in a consistent rise of about an additional 25% increase in the fracture energy for the concentrations investigated at, and below, 1.0 wt%. However, a further increase in the concentration of

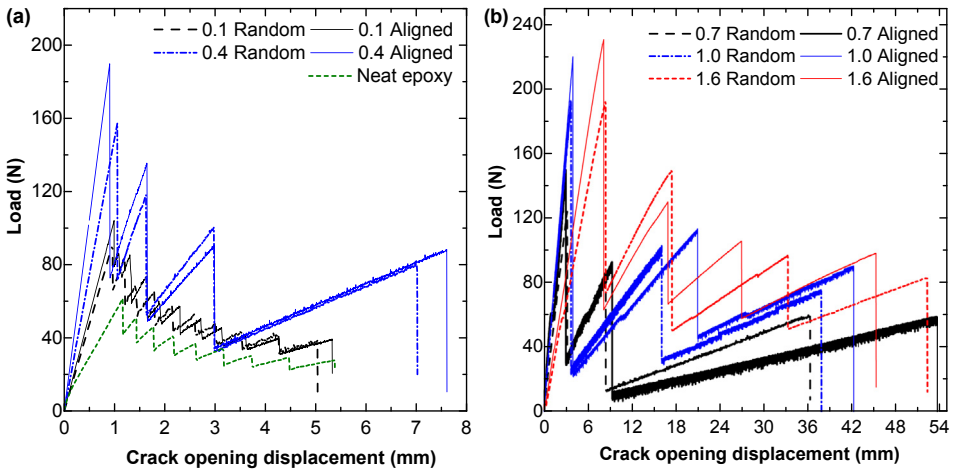

Fig. 6. Load versus displacement curves for the epoxy nanocomposites containing different concentrations of CNFs and for both randomly-oriented or aligned CNFs in the epoxy nanocomposite layer.

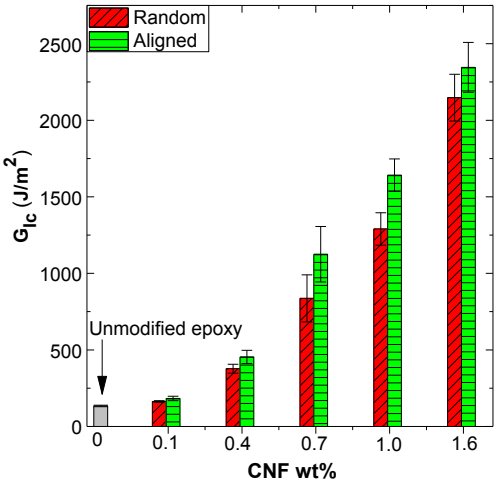

Fig. 7. Values of the fracture energy, G_{IC}, for the epoxy nanocomposites containing different concentrations of CNFs and for both randomly-oriented or aligned CNFs in the epoxy nanocomposite layer.

the CNFs to 1.6 wt% showed a relatively small difference between the fracture energies of the aligned and randomly-oriented CNF nanocomposites which was not statistically significant. Similar observations have been reported for CNT/epoxy nanocomposites at relatively high concentrations of CNTs, and were suggested to be due to the lack of free space available for the rotation and alignment of the CNTs in the epoxy when a relatively high concentration of nanofiller was present [16]. The toughening mechanisms responsible for these observed improvements in the measured toughness are discussed in the following section.

3.4. Toughening mechanisms

Post-failure examination of the fracture surfaces of the DCB samples gave an insight into the toughening mechanisms responsible for the improvements in the fracture energy of the epoxy nanocomposites. A typical featureless and smooth fracture surface was observed for the unmodified epoxy which was indicative of a very brittle fracture. Fig. 8 shows a photograph of the fracture surface for a nanocomposite sample where the regions of crack initiation and arrest are visible as curved lines across the width of the sample. In the epoxy layer of the DCB test, crack growth occurred under predominantly plane-strain conditions but with plane-stress conditions at the specimen edges of the specimen, causing the curved profile of the crack front. There is a distinct whitening of the polymer along these crack initiation/arrest lines. Examination of these regions using the SEM revealed a pattern of tear marks, which provides evidence of plastic deformation in the epoxy polymer along the line of crack initiation, which would have occurred immediately before the onset of the rapid growth of the crack. Further away from the stress-whitened regions, where the crack had propagated rapidly, there was very little evidence of ductile, plastic deformation, and the glassy fracture surface was representative of a very brittle fracture having occurred.

Fig. 8. Photograph of the crack fronts on the fracture surface of an epoxy nanocomposite with 1.0 wt% aligned CNFs.

Fig. 9 shows SEM micrographs of the stress-whitened region which correspond to the location of the onset of crack growth (i.e. the crack initiation location, see the inset in Fig. 8) in the epoxy nanocomposites containing different concentrations of aligned CNFs. Patterns of tear marks were observed in most of these images, revealing the plastic deformation of the epoxy that had occurred in the stress-whitened regions, either just ahead of the crack tip or due to some extent of slow crack growth occurring prior rapid crack growth taking place. The size and roughness of the stress-whitened region both increased with CNF concentration. The increase in the severity of the tear marks and the roughness with increasing CNF concentration is indicative of the increased plastic deformation of the epoxy in the process zone ahead of the crack tip due to the presence of the CNFs. As shown in Fig. 9, a significant number of CNFs were pulled out of the epoxy, leaving behind a void on the opposite crack surface. The areal density of the pulled-out regions of the CNFs increased with the increasing concentration of aligned CNFs. Moreover, some of the CNFs showed evidence of having experienced uncoiling and a cup-cone type of failure. This uncoiling phenomenon is unique to CNFs due to their stacked graphene cup morphology [22], which has been previously observed using TEM, revealing an uncoiled nanoribbon of graphene sheet [45]. The uncoiling and cup-cone type failure of CNFs was observed for both aligned and randomly-oriented CNF epoxy nanocomposites. However, the fibre pull-out mechanism is typically the most dominant mechanism in increasing the fracture energy [2]. The increase in the fracture energy during pull-out is due to the work of friction by the interfacial shear stress between the CNFs and the epoxy polymer. During this pull-out process the CNFs also formed a bridging zone behind the crack tip. This is evident from SEM observations of the crack bridging by CNFs, as shown in Fig. 10. The average length of the CNFs bridging the crack at its maximum opening displacement was about 8 μm. The bridging density of the CNFs decreased with decreasing concentration of CNFs, with almost no bridging being observed for the 0.1 wt% CNF epoxy nanocomposite samples. In order to pull-out and bridge the crack, the CNF must firstly debond from the epoxy. The strain energy absorbed in overcoming the adhesion of the epoxy/CNF interface during the debonding process would also increase the fracture energy, but to a lesser extent. If the interfacial bond strength exceeds the strength of the nanofibres, the CNFs would rupture prematurely before pull-out occurred. However, the rupture of the CNFs would result in smaller improvements in the values of the fracture energy, since the strain energy consumed during fibre rupture is reported to be significantly lower than that pertinent to pull-out [46].

Further, a significant number of relatively large voids are present around the CNFs (see Fig. 9c–f) and are indicative of plastic void growth of the epoxy polymer in the process zone, which leads to an additional increase in the fracture energy, compared to the unmodified epoxy. This arises because in the process zone ahead of the crack tip, where a triaxial stress-field exists, the CNFs debond from the epoxy as the local stresses increase at the crack tip. The debonded CNFs act as voids in the epoxy which allows the polymer to deform plastically, and so the voids increase in size. For rubber- and nanosilica-toughened epoxies, this plastic void growth mechanism has been shown to significantly increase the fracture toughness of the material [23,47].

Therefore, the aggregate increase in the fracture energy of the epoxy due to the addition of the CNFs is considered to be a combination of the energy dissipated by (a) the frictional energy associated with the CNFs now pulling-out from the epoxy, (b)

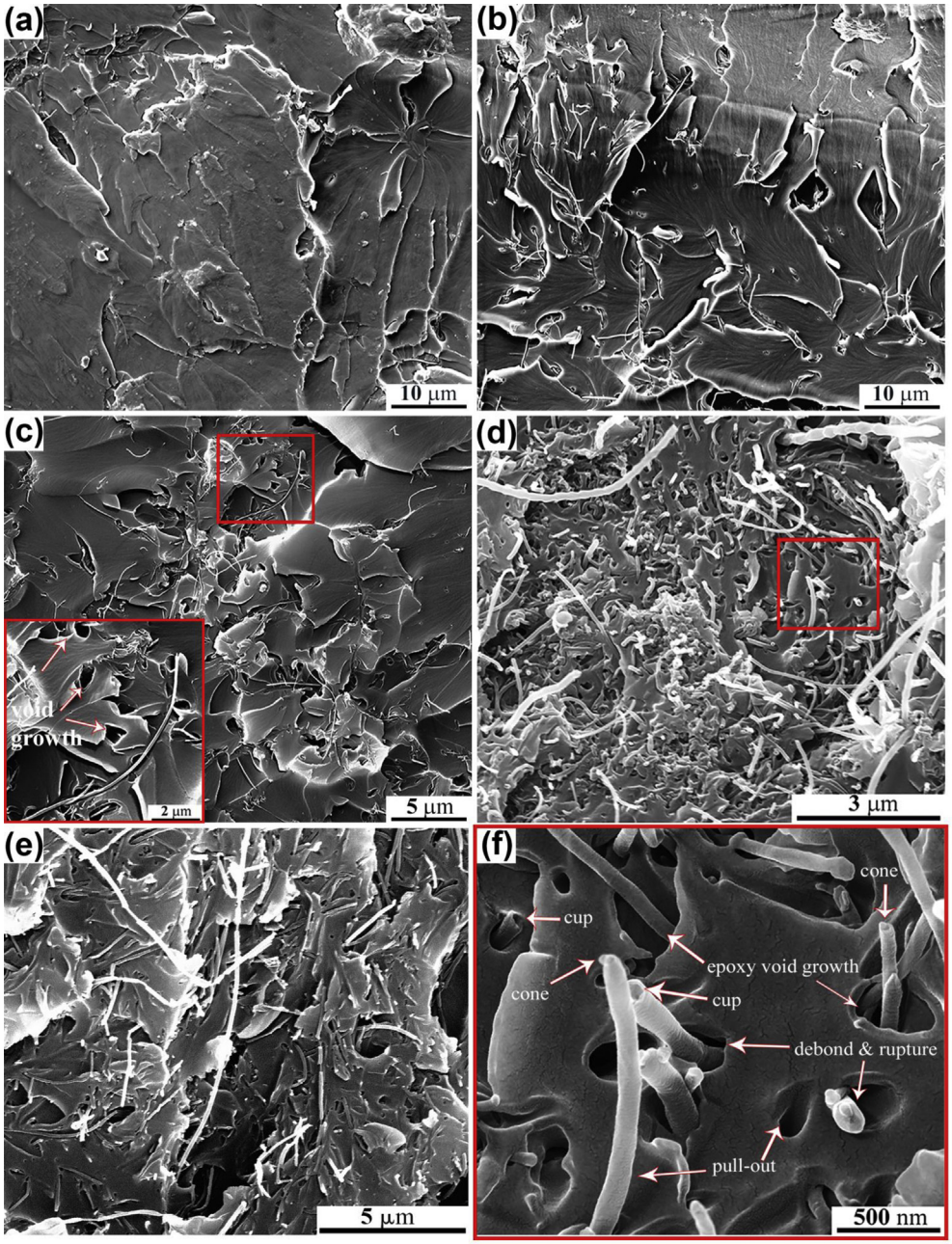

Fig. 9. SEM images of the crack initiation region of the fracture surfaces for the epoxy nanocomposites containing aligned CNFs of concentration; (a) 0.1 wt%; (b) 0.4 wt%; (c) 0.7 wt %; (d) 1.0 wt%; (e) 1.6 wt% and (f) is of the inset of (d) at a higher magnification for the 1.0 wt% nanocomposite.

rupture of CNFs, (c) interfacial debonding of the CNFs from the epoxy, and (d) void growth of the epoxy which initiates from the hole created by the debonded CNFs.

Considering the alignment of the CNFs perpendicular to the crack path in the nanocomposites, such alignment of the CNFs would lead to a higher fraction of CNFs participating in the above toughening mechanisms. For a random orientation of CNFs in the epoxy, the probability of the crack front encountering the CNFs depends on their orientation angle. For short fibre composites with a random fibre orientation, this probability is given by $\cos\theta$ (refer to Fig. 4 for the orientation axes), and for an orientation angle above 60° the probability is less than 50% [27,48]. This would lead to a lower fraction of CNFs involved in the pull-out, bridging and rupturing mechanisms for the epoxy nanocomposites containing the randomly-oriented CNFs. This is clearly evident for the randomly-oriented materials, as is shown in Fig. 11a, where a greater number of CNFs which were oriented parallel to the crack path have undergone debonding but without participating in the pull-out or void growth toughening mechanisms. While for the aligned epoxy nanocomposites, as shown in Fig. 11b, almost all the CNFs have now undergone debonding and pull-out, and hence led to the void growth mechanism being operative. In addition, if aligned normal to the direction of crack growth, the CNFs are far more likely to bridge the crack faces and undergo tensile rupture as the crack tip advances, as may be seen from comparing Fig. 10c and d.

3.5. Theoretical modelling of the fracture energy

As discussed in the previous section, the primary toughening mechanisms in the epoxy nanocomposites based on the

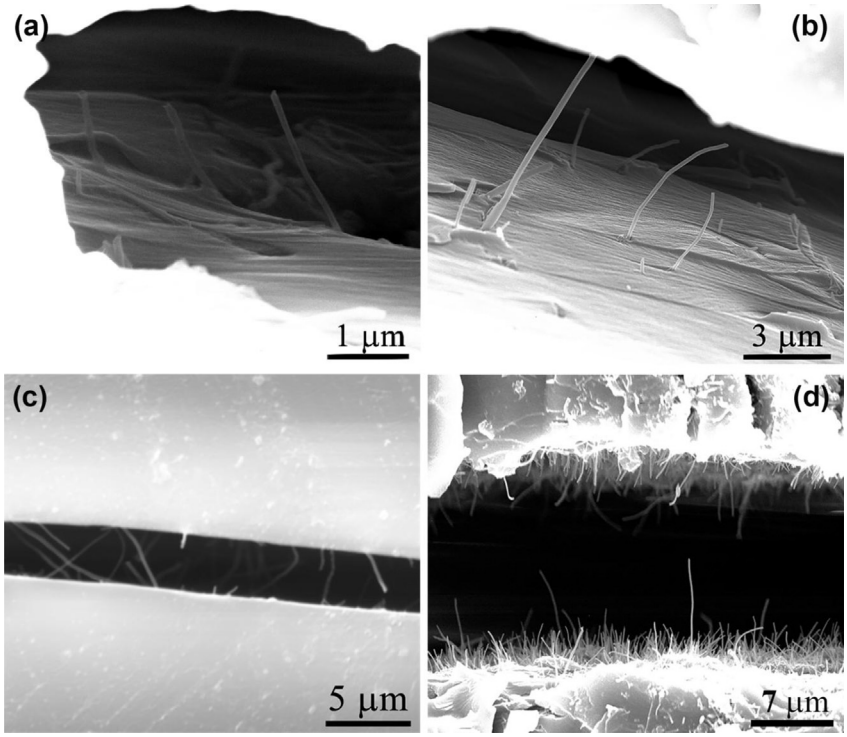

Fig. 10. SEM images of CNFs bridging the crack in epoxy nanocomposites. (a) '0.4 random'; (b) '0.4 aligned'; (c) '0.7 random'; and (d) '1.0 aligned'.

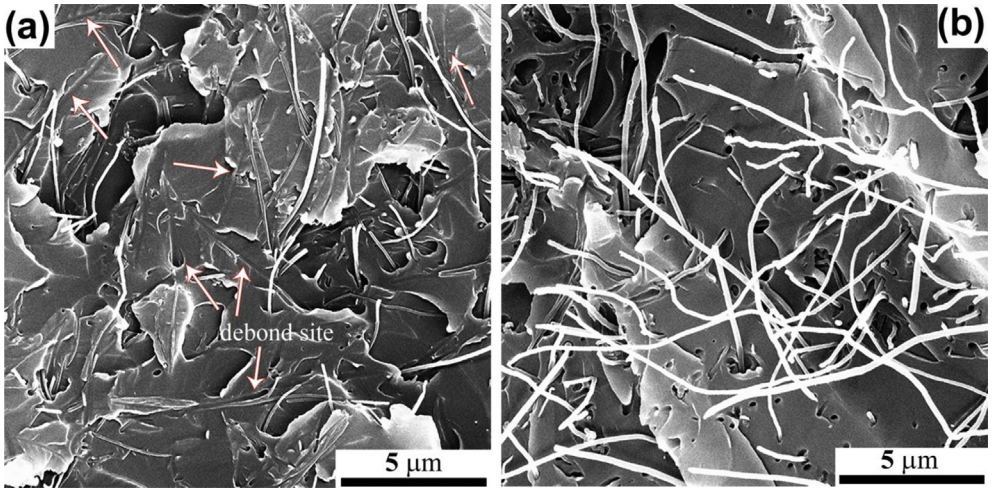

Fig. 11. Comparison of the pull-out of CNFs in the epoxy nanocomposites for (a) '1.0 random' and (b) '1.0 aligned' samples.

fractographic evidence were debonding and pull-out of the CNFs, plastic void growth of the epoxy initiated by the voids formed by the CNFs debonding and the CNFs bridging and finally rupturing across the crack faces behind the advancing crack tip. Assuming the application of continuum mechanics is valid at the nanoscale and the interfacial stress being constant [15,49], the energy dissipated by fibre pull-out based on the conventional expression from Hull [50] and Cottrell-Kelly [see 2] is given by:

$$\Delta G_{\text{pull-out}} = \frac{N_{\text{po}} \pi d_{\text{f}} \tau_{\text{i}} l_{\text{po}}^2}{2} \tag{2}$$

where l_{po} is the nanofibre pull-out length, d_f is the diameter of the CNF, τ_{i} is the interfacial shear strength and N_{po} is the total number of nanofibres per unit area of crack surface. N_{po} is related to the volume fraction, V_{fpo}, of CNFs which are pulled-out from the epoxy:

$$N_{\text{po}} = \frac{\text{nanofibre volume}}{\text{volume per nanofibre}} = \frac{l_{\text{f}} V_{\text{fpo}}}{l_{\text{f}} A_{\text{f}}} = \frac{V_{\text{fpo}}}{A_{\text{f}}} \tag{3}$$

where A_{f} is the nanofibre cross-sectional area and l_{f} is the nanofibre length. For a given weight fraction of CNFs in the epoxy, not all of the CNFs are involved in the pull-out process. Therefore, the volume fraction of CNFs pulled-out from the epoxy V_{fpo} has been determined by counting from the SEM micrographs the number of CNFs on the fracture surface. A total of sixteen SEM micrographs were used per sample type to determine the CNF pull-out volume fraction. Previous studies have successfully demonstrated the use of a similar approach to analytically calculate the strength [51] and

toughness [15] of CNT containing polymer composites. (Note: the CNF pull-out count from the fracture surfaces also includes the voids left behind by the CNFs pulled-out onto the opposite crack face). Substituting Eq. 3 into 2 gives:

$$\Delta G_{\text{pull-out}} = \frac{2V_{\text{fpo}}\tau_i l_{\text{po}}^2}{d_f} \tag{4}$$

The CNF pull-out length is difficult to determine with accuracy from SEM images of the fracture surfaces, particularly for samples with a relatively high volume fraction of CNFs. Also, relatively long CNFs are expected to rupture at the crack plane, since their embedded lengths on either side of the crack plane are long enough for the stress in the CNF to build up sufficiently to break them. Two outcomes are possible depending on the length of the embedded CNFs: (a) the CNFs pull-out when the length is shorter than the critical length given by the classical Kelly-Tyson [2,52] formula i.e. $l_c = \sigma_f d_f / 2\tau_i$, or (b) the CNFs rupture when their length is longer than the critical length. The longest possible pull-out length of the CNFs is equal to half the critical length of the CNFs embedded in the nanocomposites as given by the Kelly-Tyson formula:

$$l_{\text{po}} = \frac{\sigma_f d_f}{4\tau_i} \tag{5}$$

where σ_f is the nanofibre strength. Substituting Eq. 5 into 4 gives the estimate of the pull-out energy in terms of the inherent properties of the nanocomposite as follows:

$$\Delta G_{\text{pull-out}} = \frac{V_{\text{fpo}}\sigma_f^2 d_f}{8\tau_i} \tag{6}$$

A wide range of values for the interfacial shear strength between CNFs and epoxies have been reported in the literature, [53,54]. However, the maximum possible interface strength between the epoxy and CNFs is limited by the shear strength of the epoxy polymer. From Table 1 the shear strength of the epoxy polymer may be taken to be half that of the tensile yield strength using Tresca yield criterion, giving a value of 25 MPa. This value is used to estimate the contribution to the fracture energy from pull-out of the CNFs.

The contribution to the fracture energy due to CNF bridging is from the energy required to pull-out the bridging CNFs from the epoxy, and is therefore accounted by $\Delta G_{\text{pull-out}}$ [46]. Whereas, the energy contribution due to the elastic deformation of the CNFs prior to rupturing, whether in the plastic zone ahead of the crack tip or in its wake, is given by Ref. [27]:

$$\Delta G_{\text{rupture}} = \frac{V_{\text{fpo}}\sigma_f\, l_f\, \varepsilon_{\max}}{2} = \frac{V_{\text{fpo}}\sigma_f^2\, l_f}{2\, E_f} \tag{7}$$

where E_f and $\varepsilon_{\max}$ are the Young's modulus and the tensile failure strain of the CNFs, respectively.

The CNFs undergo debonding prior to the pull-out process. The interfacial debonding of the CNFs is an essential process because it allows them to pull-out and initiates plastic void growth of the epoxy around the hole so created. The interfacial debonding energy, ΔG_{db}, is given by Refs. [15,50]:

$$\Delta G_{\text{db}} = \frac{V_f l_{\text{po}} G_i}{d_f} \tag{8}$$

where G_i is the interfacial fracture energy between the CNFs and the epoxy. Ozkan et al. [53]. measured the interfacial fracture energy between CNFs and an epoxy polymeric matrix to be 3.3 J/m^2, and this value was used in the present study.

In addition to the CNF pull-out mechanism, the plastic void growth of the epoxy matrix promoted by debonding of CNFs from the epoxy matrix would further increase the fracture energy. In previous studies [23,47], the plastic void growth mechanism was quantitatively shown to significantly improve the fracture toughness of a nanosilica modified epoxy polymer. Huang and Kinloch [55] have shown that the fracture energy, ΔG_v, contribution from the plastic void growth mechanism can be calculated as follows:

$$\Delta G_v = \left(1 + \frac{\mu_m}{\sqrt{3}}\right)^2 \left(V_{\text{void}} - V_{\text{fpo}}\right)\sigma_y r_{yu} K_{vm}^2 \tag{9}$$

where V_{void} is the volume fraction of the voids and μ_m is a material constant allowing for the pressure dependency of the yield stress. The parameter K_{vm} is the maximum stress concentration for the von Mises stresses around a debonded CNF, which lies between 2.11 and 2.12 [15]. The parameters σ_y and r_{yu} are respectively the tensile yield stress and the plastic zone size at fracture of the unmodified epoxy. The plastic zone size is given by:

$$r_{yu} = \frac{1}{6\pi}\frac{E_m G_{CU}}{(1-\nu^2)\sigma_y^2} \tag{10}$$

where G_{cu} is the fracture energy, E_m is the tensile modulus and ν is the Poisson's ratio of the unmodified epoxy polymer. Each void is assumed to be a truncated cone with the smaller diameter equal to the diameter of the CNFs and the larger void diameter is determined from the SEM micrographs which has a varying distribution depending on the size of the CNFs. In the present study the void diameter was estimated from SEM micrographs to be approximately seven times the diameter of the CNFs around which the void

Table 1
List of values for the various parameters used in the analytical modelling study.

Parameter	Symbol	Unit	Value	Source
CNF diameter	d_f	nm	135	[35]
CNF average length after dispersion	l_f	μm	20	This study
CNF strength	σ_f	GPa	8.7	[35]
Young's modulus of the CNF	E_f	GPa	320	[56]
Density of the CNF	ρ_f	kg/m^3	1400	[35]
Density of unmodified epoxy	ρ_m	kg/m^3	1011	[57]
CNF/epoxy interface fracture energy	G_i	J/m^2	3.3	[53]
Tensile yield strength of unmodified epoxy	σ_y	MPa	50.5	[57]
Young's modulus of unmodified epoxy	E_m	GPa	3.17	[57]
Pressure dependent yield stress constant	μ_m	–	0.2	[55]
Maximum von Mises stress concentration	K_{vm}	–	2.11	[15]

are formed. In other words, $V_{void} = 16V_{fpo}$ in the present case. Therefore, the fracture energy, G_{Ic}, of the CNF toughened epoxy can be expressed as:

$$G_{Ic} = G_{CU} + \Delta G_{rupture} + \Delta G_{pull\text{-}out} + \Delta G_{db} + \Delta G_{v} \quad (11)$$

The above model is used to estimate the fracture energy improvement by considering an average CNF diameter equal to 135 nm as supplied by the manufacturer [53].

Equations (6), (8) and (9) show that the energy contributions due to CNF pull-out, debonding and epoxy void growth depend strongly on the diameter of the nanofibres. The probability density function of CNF diameter is shown in Fig. 2c. The 135 nm diameter value provided by the manufacturer corresponds to the median of this distribution. By accounting for the distribution of the CNF diameter, the total fracture energy can be expressed in terms of the diameter probability function $\rho(d_f)$:

$$G_{Ic} = G_{CU} + \Delta G_{rupture} + \int_{d_{min}}^{d_{max}} \left(\Delta G_{pull\text{-}out} + \Delta G_{db} + \Delta G_{v}\right)\rho\left(d_f\right)\mathrm{d}d_f \quad (12)$$

where $\Delta G_{rupture}$ is independent of the CNF diameter as can be seen from Eq. (7). The fracture energy modelling results are calculated from the experimentally-determined values of V_{fpo} for the random and aligned nanocomposite, apart from the '1.6 aligned' nanocomposite. Due to the relatively high concentration of CNFs in the 1.6 wt% nanocomposite, it is excessively time consuming to count the number of CNFs pulled out on the crack surface.

The fracture energy is also calculated by assuming all the CNFs are pulled out, hence $V_{fpo} = V_f$. The V_f is estimated from the CNF weight fraction by considering the graphitic CNF wall density to be 1400 kg/m^3 [35]. This approach assumes that all the CNFs in a unit volume of epoxy are intersected by the advancing crack. The values of all the input parameters used to calculate the fracture energy of the epoxy polymers containing the CNFs are given in Tables 1 and 2 Model predictions and comparison with experimental results are presented in the following section.

3.6. Results of theoretical models

Fig. 12 shows the results from the theoretical modelling studies compared to the experimentally measured values of G_{Ic}. The figure shows two curves calculated using the model assuming that the CNFs have the mean diameter (Eq. (11)) or the diameter varies according to the probability density function (Eq. (12)). The toughness values are slightly higher when it is assumed that all the CNFs have the same (mean) diameter. Good agreement can be seen between the experimental results and the predicted fracture energies which supports the primary toughening mechanisms which have been proposed for the epoxy polymers modified using randomly-oriented or aligned CNFs. The CNF pull-out and the epoxy void growth were the two most dominant toughening mechanisms, accounting for the majority of the fracture energy enhancement for all the epoxy nanocomposites.

Table 2
Measured values of the volume fraction, V_{fpo}, of CNFs which are pulled-out from the epoxy and the volume fraction, V_{void}, of the voids formed around the debonded CNFs.

CNFs (wt%)	V_f (%)	V_{fpo} (%)		V_{void} (%)	
		Aligned	Random	Aligned	Random
0.1	0.08	0.02	0.01	0.32	0.23
0.4	0.33	0.23	0.18	3.99	3.34
0.7	0.58	0.53	0.43	9.39	8.12
1.0	0.82	0.78	0.63	13.76	11.91
1.6	1.31	–	–	–	–

Table 3a shows a comparison of the highest fracture toughness improvements that have been reported in the literature for CNT and CNF modified epoxies against the nanocomposites studied here. It is noteworthy that the toughness improvements achieved in the present study are many times higher than those reported previously. These variations in the enhancement of the fracture energy may be mainly explained by the differences in the length of the CNFs, and its effect on the fracture energy due to pull-out of the CNFs as given by Eq. (4). For example, if the CNF length is reduced to 6 μm, as was the case in the study by Palmeri et al. [22], the fracture energy due to pull-out will be greatly reduced. In order to obtain a better estimate for such an effect, and for the purpose of comparison between the two studies, it has been assumed that the volume fraction of CNFs that are pulled-out is only dependent on the concentration of CNFs and is independent of the length. On this basis, for the 0.7 wt% of random CNF nanocomposite studied by Palmeri et al. [22], assuming that all the modelling parameters (besides the value of the nanofibre length, l_f) are similar in value to those used in the present work, the expected improvement in the value of the fracture energy, as given by Eq. (11) with a CNF length equal to 6 μm, would be about 116%. This is very similar to the measured improvement reported in their study, see Table 3a. The improvements in the fracture energy of epoxy polymer containing CNFs reported in some other studies can be similarly estimated and the data are given in Table 3b where the matrix properties are taken from Ref. [58]. Using Eqs. (11) or (12) and the relevant data in Tables 1 and 3b, the proposed model gives a reasonable estimate for the measured values of G_{Ic} reported previously in the literature, as may be seen from Table 3a. It is also clear that the improvement in the fracture energy of the epoxy due to the addition of the CNFs or CNTs is strongly dependent on the dimensions of the nanofiller, especially the fibre length. Thus, the use of longer CNFs, as in the present study, would indeed be expected to lead a better enhancement in the fracture energy of the epoxy nanocomposites.

4. Conclusions

The fracture energy and electrical conductivity of a thermoset epoxy polymer modified by the addition of carbon nanofibres (CNFs) have been investigated. The CNFs were dispersed in a liquid epoxy resin using a surfactant and then processed employing a three-roll mill to give a good degree of dispersion with the majority of the CNFs having lengths of between 16 and 24 μm. An AC electric field has been found to be very effective in aligning CNFs to form a chain-like structure in epoxy with the majority (85%) of the CNFs lying within ±15° of the applied electric field. The alignment of 0.4 wt% of CNFs in the epoxy nanocomposite led to the formation of a percolating network of CNFs which yielded a measurable DC conductivity, while simultaneously increasing the average fracture energy, G_{Ic}, from 134 J/m^2 to 453 J/m^2, compared to the unmodified epoxy polymer. The highest increases in toughness and conductivity were for the epoxy nanocomposites containing 1.6 wt% of aligned CNFs. The fracture energy and the electrical conductivity of this nanocomposite were increased by about 1600% (from 134 to 2345 J/m^2) and seven orders of magnitude above the unmodified epoxy. When compared to randomly-oriented CNFs, the alignment of the CNFs resulted in a 27% increase in the fracture energy and about a five-fold increase in the electrical conductivity at 1.0 wt% of CNFs. The main toughening mechanisms which led to the increase in the fracture

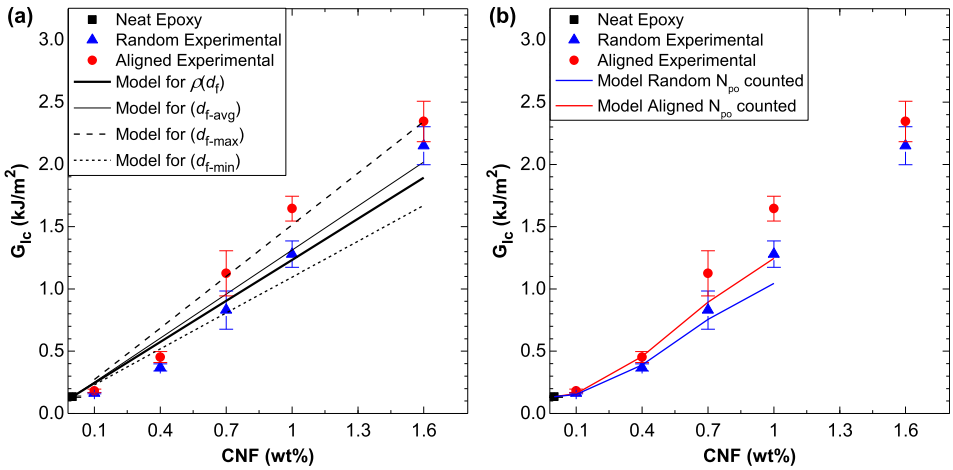

Fig. 12. Comparison of the experimental and theoretically calculated fracture energies as a function of the concentration of CNFs. (a) Model calculations based on total volume fraction ($V_{fpo} = V_f$) using minimum, mean, maximum, and probabilistic distribution of the CNF diameter; and (b) model calculations based on the experimentally measured V_{fpo} for random- and aligned-CNF nanocomposites.

Table 3a
Fracture toughness, G_{Ic}, values of epoxy polymers toughened with 1-D carbon nanofillers.

Source	Nanofiller	Nanofiller concentration (wt%)	Improvement (%)	Model prediction (%)
The present study	CNFs-Random	1.6	1500	1410
	CNFs-Random	1.0	850	880
	CNFs-Random	0.7	500	610
	CNFs-Random	0.4	180	350
Tang et al. [21]	MWCNTs*	1.0	130	–
Palmeri et al. [22]	CNFs	0.68	113	95
Liu et al. [19]	CNFs	0.4	80	140
Hsieh et al. [15]	CNTs	0.5	70	60

*Multiwall carbon nanotubes (MWCNTs).

Table 3b
Parameters used to calculate the fracture energy improvement in Table 3a using the theoretical model from Section 3.5 for the different studies from the literature.

Source	Nanofiller	τ_i (MPa)	l_f (μm)	d_f (nm)
Palmeri et al. [22]	CNFs	36 (Ref [58])	6	135
Liu et al. [19]	CNFs	36 (Ref [58])	20	135
Hsieh et al. [15]	CNTs	47	120	120

energy for the nanocomposites were identified to be (a) interfacial debonding of the CNFs from the epoxy, (b) the energy associated with the pull-out of CNFs from the epoxy, (c) void growth of the epoxy which initiates from the hole created by the debonded CNFs, and (d) the rupturing of CNFs. The alignment of CNFs perpendicular to the crack path generally led to a higher fraction of CNFs participating in the above toughening mechanisms, and thus accounted for the relatively higher values of G_{Ic} typically measured for these nanocomposites, compared to those containing randomly-oriented CNFs.

Acknowledgements

The authors kindly acknowledge Mr Geoffrey Thomas (RMIT) for providing access to the HP impedance analyzer and the technical assistance of Mr Peter Tkatchyk (RMIT) as well as the RMIT Microscopy and Microanalysis Facility (RMMF) team. The authors are thankful for the financial support received from the Australian Research Council's Discovery Grant Program (DP140100778).

References

[1] A.J. Kinloch, Adhesives in engineering, in: Proceedings of the Institution of Mechanical Engineers, 1997, pp. 307–336, http://dx.doi.org/10.1243/0954410971532703. Part G.
[2] J.K. Kim, Y.W. Mai, High strength, high fracture toughness fibre composites with interface control-a review, Compos. Sci. Technol. 41 (1991) 333–378.
[3] C. Bucknall, I. Partridge, Phase separation in epoxy resins containing polyethersulphone, Polymer 24 (1983) 639–644, http://dx.doi.org/10.1016/0032-3861(83)90120-9.
[4] D.J. Hourston, J.M. Lane, The toughening of epoxy resins with thermoplastics: 1. Trifunctional epoxy resin-polyetherimide blends, Polymer 33 (1992) 1379–1383.
[5] W.D. Bascom, R.L. Cottington, R.L. Jones, P. Peyser, The fracture of epoxy and elastomer modified epoxy polymers in bulk and as adhesives, J. Appl. Polym. Sci. 19 (1975) 2545–2562.
[6] A.J. Kinloch, S.J. Shaw, D.A. Tod, D.L. Hunston, Deformation and fracture behaviour of a rubber-toughened epoxy: 1. Microstructure and fracture studies, Polymer 24 (1983) 1341–1354, http://dx.doi.org/10.1016/0032-3861(83)90070-8.
[7] W. Bauhofer, J.Z. Kovacs, A review and analysis of electrical percolation in carbon nanotube polymer composites, Compos. Sci. Technol. 69 (2009) 1486–1498, http://dx.doi.org/10.1016/j.compscitech.2008.06.018.
[8] E.T. Thostenson, Z. Ren, T.-W. Chou, Advances in the science and technology of carbon nanotubes and their composites: a review, Compos. Sci. Technol. 61 (2001) 1899–1912, http://dx.doi.org/10.1016/S0266-3538(01)00094-X.
[9] M. Rahmat, P. Hubert, Carbon nanotube–polymer interactions in nanocomposites: a review, Compos. Sci. Technol. 72 (2011) 72–84, http://dx.doi.org/10.1016/j.compscitech.2011.10.002.
[10] M.H. Al-Saleh, U. Sundararaj, Review of the mechanical properties of carbon nanofiber/polymer composites, Compos. Part A Appl. Sci. Manuf. 42 (2011) 2126–2142, http://dx.doi.org/10.1016/j.compositesa.2011.08.005.
[11] G.G. Tibbetts, M.L. Lake, K.L. Strong, B.P. Rice, A review of the fabrication and properties of vapor-grown carbon nanofiber/polymer composites, Compos. Sci. Technol. 67 (2007) 1709–1718, http://dx.doi.org/10.1016/j.compscitech.2006.06.015.
[12] S. Shadlou, E. Alishahi, M.R. Ayatollahi, Fracture behavior of epoxy nanocomposites reinforced with different carbon nano-reinforcements, Compos.

Struct. 95 (2013) 577–581, http://dx.doi.org/10.1016/j.compstruct.2012.08.002.
[13] M.A. Rafiee, J. Rafiee, I. Srivastava, Z. Wang, H. Song, Z.-Z. Yu, et al., Fracture and fatigue in graphene nanocomposites, Small 6 (2010) 179–183, http://dx.doi.org/10.1002/smll.200901480 (Weinheim an Der Bergstrasse, Germany).
[14] S. Chatterjee, F. Nafezarefi, N.H. Tai, L. Schlagenhauf, F.A. Nüesch, B.T.T. Chu, Size and synergy effects of nanofiller hybrids including graphene nanoplatelets and carbon nanotubes in mechanical properties of epoxy composites, Carbon 50 (2012) 5380–5386, http://dx.doi.org/10.1016/j.carbon.2012.07.021.
[15] T.H. Hsieh, A.J. Kinloch, A.C. Taylor, I.A. Kinloch, The effect of carbon nanotubes on the fracture toughness and fatigue performance of a thermosetting epoxy polymer, J. Mater. Sci. 46 (2011) 7525–7535, http://dx.doi.org/10.1007/s10853-011-5724-0.
[16] S.U. Khan, J.R. Pothnis, J.-K. Kim, Effects of carbon nanotube alignment on electrical and mechanical properties of epoxy nanocomposites, Compos. Part A Appl. Sci. Manuf. 49 (2013) 26–34, http://dx.doi.org/10.1016/j.compositesa.2013.01.015.
[17] B. Fiedler, F.H. Gojny, M.H.G. Wichmann, M.C.M. Nolte, K. Schulte, Fundamental aspects of nano-reinforced composites, Compos. Sci. Technol. 66 (2006) 3115–3125, http://dx.doi.org/10.1016/j.compscitech.2005.01.014.
[18] F. Gojny, M. Wichmann, B. Fiedler, K. Schulte, Influence of different carbon nanotubes on the mechanical properties of epoxy matrix composites – A comparative study, Compos. Sci. Technol. 65 (2005) 2300–2313, http://dx.doi.org/10.1016/j.compscitech.2005.04.021.
[19] W. Liu, J. Kong, W.E. Toh, R. Zhou, G. Ding, S. Huang, et al., Toughening of epoxies by covalently anchoring triazole-functionalized stacked-cup carbon nanofibers, Compos. Sci. Technol. 85 (2013) 1–9, http://dx.doi.org/10.1016/j.compscitech.2013.05.009.
[20] H. Miyagawa, L.T. Drzal, Effect of oxygen plasma treatment on mechanical properties of vapor grown carbon fiber nanocomposites, Compos. Part A Appl. Sci. Manuf. 36 (2005) 1440–1448, http://dx.doi.org/10.1016/j.compositesa.2005.01.027.
[21] L. Tang, H. Zhang, J. Han, X. Wu, Z. Zhang, Fracture mechanisms of epoxy filled with ozone functionalized multi-wall carbon nanotubes, Compos. Sci. Technol. 72 (2011) 7–13, http://dx.doi.org/10.1016/j.compscitech.2011.07.016.
[22] M.J. Palmeri, K.W. Putz, L.C. Brinson, Sacrificial bonds in stacked-cup carbon nanofibers: biomimetic toughening mechanisms for composite systems, ACS Nano 4 (2010) 4256–4264, http://dx.doi.org/10.1021/nn100661a.
[23] T.H. Hsieh, A.J. Kinloch, K. Masania, A.C. Taylor, S. Sprenger, The mechanisms and mechanics of the toughening of epoxy polymers modified with silica nanoparticles, Polymer 51 (2010) 6284–6294, http://dx.doi.org/10.1016/j.polymer.2010.10.048.
[24] T.H. Hsieh, A.J. Kinloch, K. Masania, J. Sohn Lee, A.C. Taylor, S. Sprenger, The toughness of epoxy polymers and fibre composites modified with rubber microparticles and silica nanoparticles, J. Mater. Sci. 45 (2009) 1193–1210, http://dx.doi.org/10.1007/s10853-009-4064-9.
[25] P.-C. Ma, N.A. Siddiqui, G. Marom, J.-K. Kim, Dispersion and functionalization of carbon nanotubes for polymer-based nanocomposites: A review, Compos. Part A Appl. Sci. Manuf. 41 (2010) 1345–1367, http://dx.doi.org/10.1016/j.compositesa.2010.07.003.
[26] G. Odegard, Constitutive modeling of nanotube–reinforced polymer composites, Compos. Sci. Technol. 63 (2003) 1671–1687, http://dx.doi.org/10.1016/S0266-3538(03)00063-0.
[27] V. Mirjalili, P. Hubert, Modelling of the carbon nanotube bridging effect on the toughening of polymers and experimental verification, Compos. Sci. Technol. 70 (2010) 1537–1543, http://dx.doi.org/10.1016/j.compscitech.2010.05.016.
[28] M. Monti, M. Natali, L. Torre, J.M. Kenny, The alignment of single walled carbon nanotubes in an epoxy resin by applying a DC electric field, Carbon 50 (2012) 2453–2464, http://dx.doi.org/10.1016/j.carbon.2012.01.067.
[29] A.I. Oliva-Avilés, F. Avilés, V. Sosa, A.I. Oliva, F. Gamboa, Dynamics of carbon nanotube alignment by electric fields, Nanotechnology 23 (2012) 465710, http://dx.doi.org/10.1088/0957-4484/23/46/465710.
[30] D. Shi, P. He, J. Lian, X. Chaud, S.L. Bud'ko, E. Beaugnon, et al., Magnetic alignment of carbon nanofibers in polymer composites and anisotropy of mechanical properties, J. Appl. Phys. 97 (2005) 064312, http://dx.doi.org/10.1063/1.1861143.
[31] X. Xie, Y. Mai, X. Zhou, Dispersion and alignment of carbon nanotubes in polymer matrix: a review, Mater. Sci. Eng. R Rep 49 (2005) 89–112, http://dx.doi.org/10.1016/j.mser.2005.04.002.
[32] S. Wu, R.B. Ladani, J. Zhang, A.J. Kinloch, Z. Zhao, J. Ma, et al., Epoxy nanocomposites containing magnetite-carbon nanofibers aligned using a weak magnetic field, Polymer (2015), http://dx.doi.org/10.1016/j.polymer.2015.04.080.
[33] T. Prasse, J.-Y. Cavaille, W. Bauhofer, Electric anisotropy of carbon nanofibre/epoxy resin composites due to electric field induced alignment, Compos. Sci. Technol. 63 (2003) 1835–1841, http://dx.doi.org/10.1016/S0266-3538(03)00019-8.
[34] M.H. Al-Saleh, U. Sundararaj, A review of vapor grown carbon nanofiber/polymer conductive composites, Carbon 47 (2009) 2–22, http://dx.doi.org/10.1016/j.carbon.2008.09.039.
[35] SIGMA-ALDRICH, Properties and Application of Carbon Nanofibers (CNFs) Synthesized Using Vapor Grown Carbon Fiber (VGCF) Manufacturing Technology, 2015. http://www.sigmaaldrich.com/china-mainland/zh/materials-science/nanomaterials/carbon-nanofibers.html (accessed 08.05.15).
[36] ISO. 25217:2009, Determination of the Mode I Adhesive Fracture Energy of Structural Adhesive Joints Using Double Cantilever Beam and Tapered Double Cantilever Beam Specimens, 2009. Geneva.
[37] H.D. Wagner, A. Lustiger, Optimized toughness of short fiber-based composites: the effect of fiber diameter, Compos. Sci. Technol. 69 (2009) 1323–1325, http://dx.doi.org/10.1016/j.compscitech.2009.03.008.
[38] T.B. Jones, Electromechanics of Particles, Cambridge University Press, New York, 1995, http://dx.doi.org/10.1017/CBO9780511574498.
[39] L. Benedict, S. Louie, M. Cohen, Static polarizabilities of single-wall carbon nanotubes, Phys. Rev. B 52 (1995) 8541–8549, http://dx.doi.org/10.1103/PhysRevB.52.8541.
[40] B. Kozinsky, N. Marzari, Static dielectric properties of carbon nanotubes from first principles, Phys. Rev. Lett. 96 (2006) 166801, http://dx.doi.org/10.1103/PhysRevLett.96.166801.
[41] M.P. Hughes, AC electrokinetics: applications for nanotechnology, Nanotechnology 11 (2000) 124–132, http://dx.doi.org/10.1088/0957-4484/11/2/314.
[42] A.K. Jonscher, A new understanding of the dielectric relaxation of solids, J. Mater. Sci. 16 (1981) 2037–2060, http://dx.doi.org/10.1007/BF00542364.
[43] A.K. Jonscher, The "universal" dielectric response, Nature 267 (1977) 673–679.
[44] B.M. Tyson, R.K. Abu Al-Rub, A. Yazdanbakhsh, Z. Grasley, A quantitative method for analyzing the dispersion and agglomeration of nano-particles in composite materials, Compos. Part B Eng. 42 (2011) 1395–1403, http://dx.doi.org/10.1016/j.compositesb.2011.05.020.
[45] J. Vera-Agullo, H. Varela-Rizo, J.A. Conesa, C. Almansa, C. Merino, I. Martin-Gullon, Evidence for growth mechanism and helix-spiral cone structure of stacked-cup carbon nanofibers, Carbon 45 (2007) 2751–2758, http://dx.doi.org/10.1016/j.carbon.2007.09.040.
[46] J. Blanco, E.J. Garcia, R. Guzman de Villoria, B.L. Wardle, Limiting mechanisms of mode I interlaminar toughening of composites reinforced with aligned carbon nanotubes, J. Compos. Mater. 43 (2009) 825–841, http://dx.doi.org/10.1177/0021998309102398.
[47] J.G. Williams, Particle toughening of polymers by plastic void growth, Compos. Sci. Technol. 70 (2010) 885–891, http://dx.doi.org/10.1016/j.compscitech.2009.12.024.
[48] V.C. Li, Y. Wang, S. Backer, A micromechanical model of tension-softening and bridging toughening of short random fiber reinforced brittle matrix composites, J. Mech. Phys. Solids 39 (1991) 607–625, http://dx.doi.org/10.1016/0022-5096(91)90043-N.
[49] H.D. Wagner, P.M. Ajayan, K. Schulte, Nanocomposite toughness from a pull-out mechanism, Compos. Sci. Technol. 83 (2013) 27–31, http://dx.doi.org/10.1016/j.compscitech.2013.04.017.
[50] D. Hull, An Introduction to Composite Materials. Cambridge Solid State Science Series, second ed., Cambridge University Press, Cambridge, 1996.
[51] S.-Y. Fu, Z.-K. Chen, S. Hong, C.C. Han, The reduction of carbon nanotube (CNT) length during the manufacture of CNT/polymer composites and a method to simultaneously determine the resulting CNT and interfacial strengths, Carbon 47 (2009) 3192–3200, http://dx.doi.org/10.1016/j.carbon.2009.07.028.
[52] A. Kelly, W.R. Tyson, Tensile properties of fibre-reinforced metals: copper/tungsten and copper/molybdenum, J. Mech. Phys. Solids 13 (1965) 329–350, http://dx.doi.org/10.1016/0022-5096(65)90035-9.
[53] T. Ozkan, Q. Chen, I. Chasiotis, Interfacial strength and fracture energy of individual carbon nanofibers in epoxy matrix as a function of surface conditions, Compos. Sci. Technol. 72 (2012) 965–975, http://dx.doi.org/10.1016/j.compscitech.2012.03.004.
[54] M.P. Manoharan, A. Sharma, A. Desai, M.A. Haque, C.E. Bakis, K.W. Wang, The interfacial strength of carbon nanofiber epoxy composite using single fiber pullout experiments, Nanotechnology 20 (2009) 295701–295706, http://dx.doi.org/10.1088/0957-4484/20/29/295701.
[55] Y. Huang, A.J. Kinloch, Modelling of the toughening mechanisms in rubber-modified epoxy polymers, J. Mater. Sci. 27 (1992) 2763–2769, http://dx.doi.org/10.1007/BF00540703.
[56] T. Ozkan, M. Naraghi, I. Chasiotis, Mechanical properties of vapor grown carbon nanofibers, Carbon 48 (2010) 239–244, http://dx.doi.org/10.1016/j.carbon.2009.09.011.
[57] WESTSYSTEM, 105 Resin Engineering Data, 2015. http://www.westsystem.com.au/files/products.resin_and_hardeners/west_system_r105_eng_data.pdf (accessed 18.02.15).
[58] HUNTSMAN, Araldite MY 721 Data Sheet, 2010. https://apps.huntsmanservice.com/WebFolder/ui/browse.do?pFileName=/opt/TDS/HuntsmanAdvanced Materials/English US/Long/Araldite MY721_US_e.pdf (accessed 10.05.15).